Supplementary Materials

Dynamic memristor array with multiple reservoir states for training efficient neuromorphic computing

Minseo Noh, Dongyeol Ju, Sungjun Kim

Division of Electronics and Electrical Engineering, Dongguk University, Seoul 04620, Republic of Korea

* Corresponding author: sungjun@dongguk.edu (S. Kim)

Contents:

recognition accuracy achieved with 20 consecutive epochs applied to 5 cells.

Structure	Device structure	Switching behavior	Endurance	Memory function	Synapse emulations	Multifunctional behavior	Ref
$TiW/Al_2O_3/Ta_2O_5/Ta$	Planar	Analog	NA	Volatile	NA	NA	[S1]
$Ti/TiO_2/HfO_2/Si$	Planar	Analog	10^3	Volatile	MLC, STDP	NA	[S2]
$Pt/TiO_2/ZrO_2/Pt$	Planar	Analog	10^3	Non volatile	STDP	NA	[S3]
Ag/aloe vera/FTO	Planar	Analog	10^2	Volatile	NA	Pavlov training	[S4]
$TiN/Ti/AlO_x/HfO_x/TiN$	Planar	digital	NA	Non volatile	NA	NA	[S5]
$Ti/TiO_2/Si$	Planar	Analog	NA	Non volatile	PPF	Reservoir computing	[S6]
$Pt/Al/TiO_y/TiO_x/Al_2O_3/Pt$	Crossbar-array	Analog	10^2	Volatile	EPSC, PPF, SRDP, SADP,	Pavlov training, synapse array, reservoir computing	This work

Table S1. Comparative assessment of memristive device performance in multifunctional synaptic applications with respect to prior research.

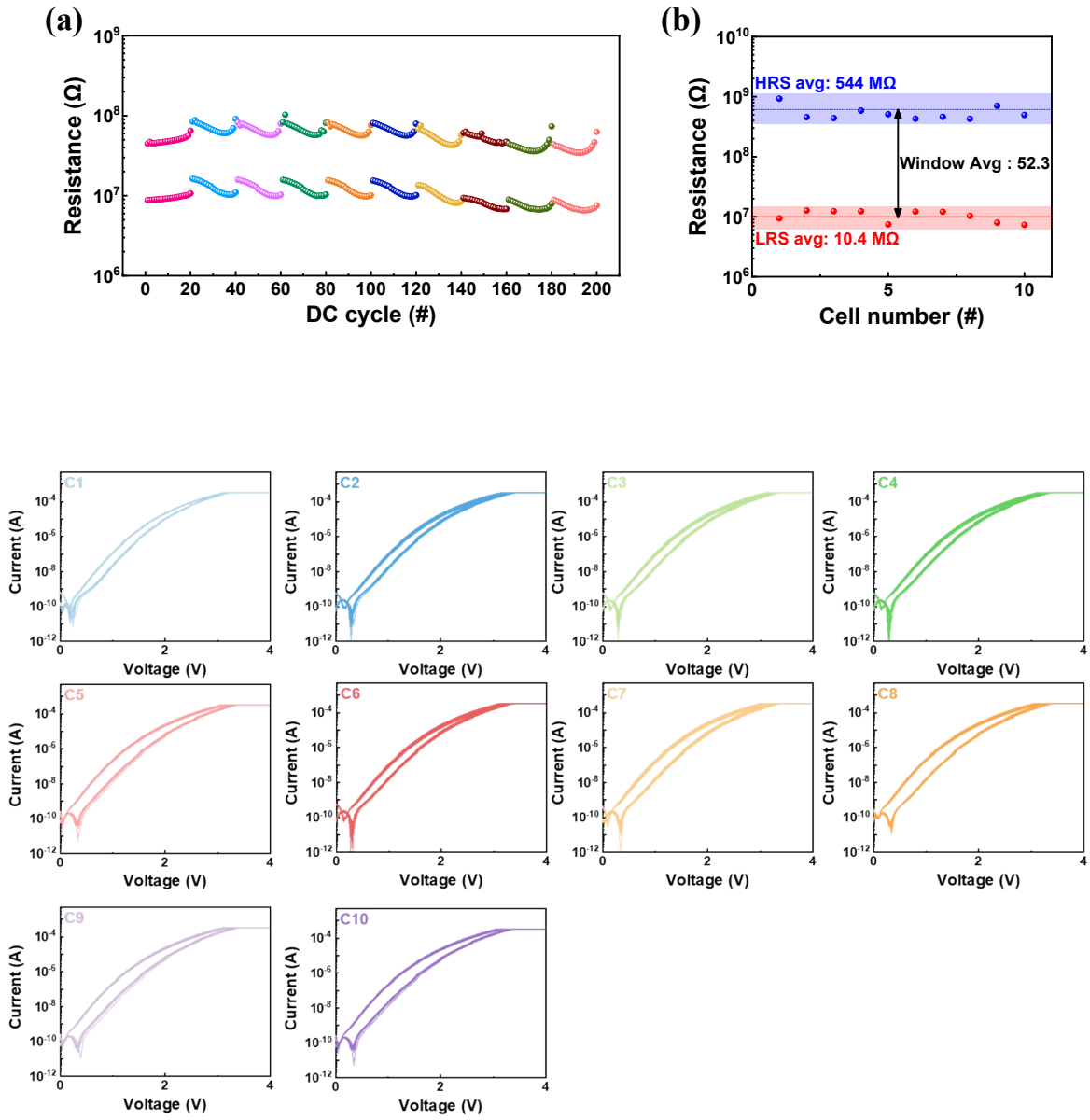

Figure S1. I-V curves acquired from 10 different cells.

Figure S2. (a) 20 cycle endurance properties of the randomly selected 10 cells. (b) The average on/off ratio of each 10 cells.

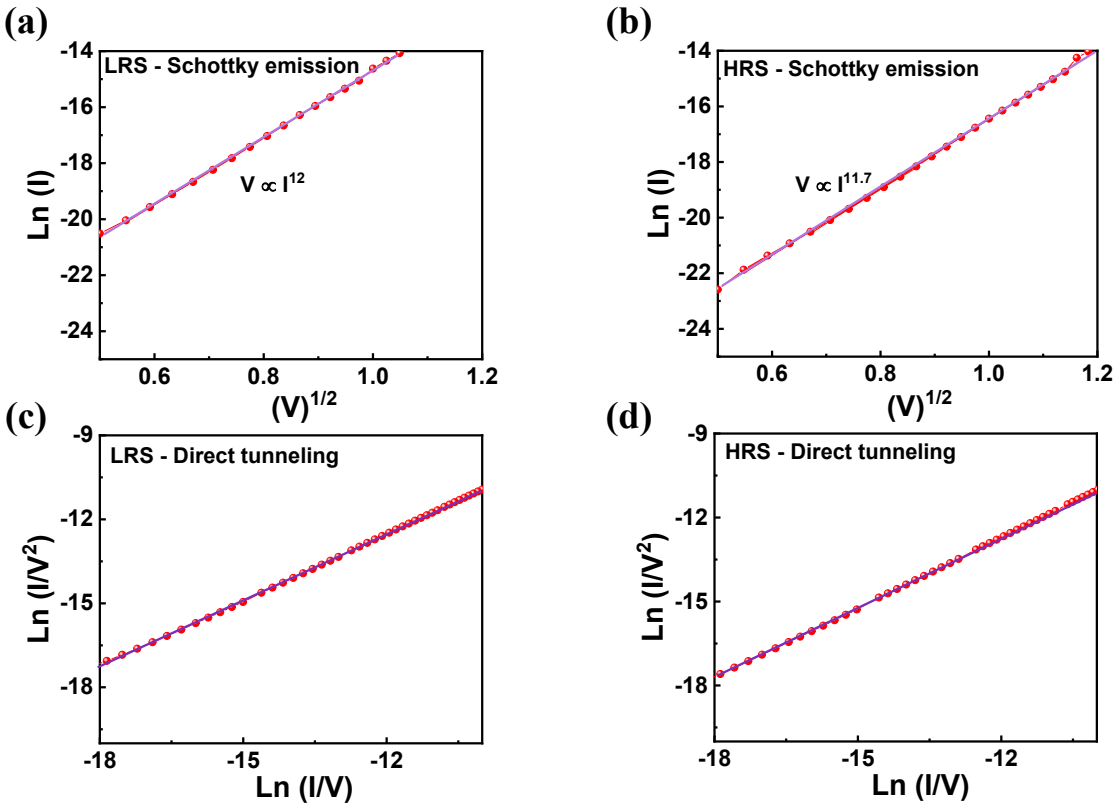

Figure S3. (a) Schottky emission conduction mechanism fitting in the LRS state of device. (b) Schottky emission conduction mechanism fitting in the HRS state of device. (c) Direct tunneling conduction mechanism fitting in the LRS state of device. (d) Direct tunneling conduction mechanism fitting in the HRS state of device.

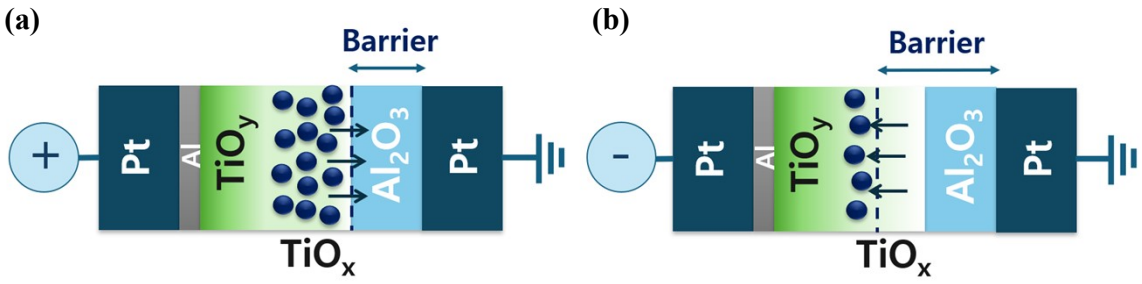

Figure S4. Illustration of conduction mechanism to explain the oxygen vacancy migration during the (a) set process and the (b) reset process.

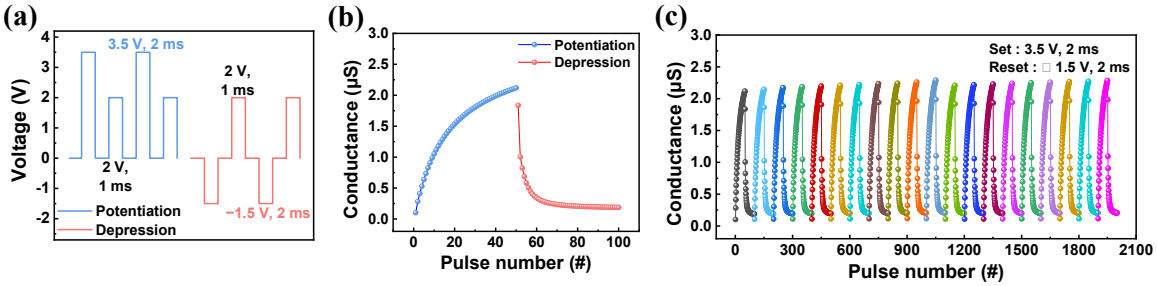

Figure S5. (a) Pulse schematics for potentiation and depression. (b) Potentiation and depression curves acquired through applied pulse schemes. (c) 20-cycle repeated potentiation and depression behavior. Potentiation pulses are composed of 50 identical set pulses at 3.5 V and 50 read pulses at 2 V. Depression pulses consist of identical reset pulses at -1.5 V and 50 read pulses at 2 V. All pulse intervals are fixed at 1 ms, and all pulse widths are set to 2 ms. Consequently, gradual increase and decrease of conductance values are observed.

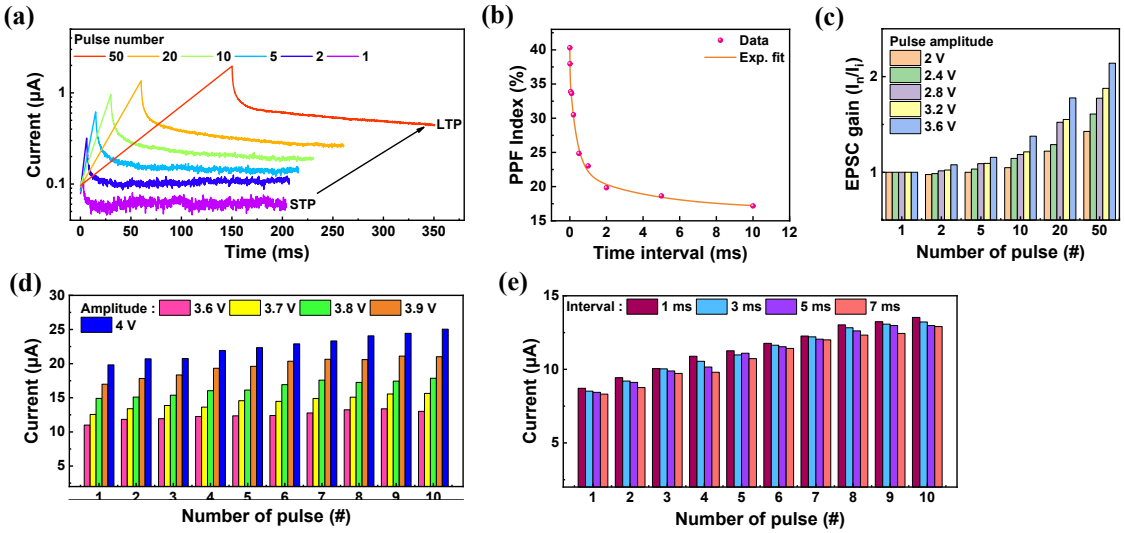

Figure S6 (a) The transition from STM to LTM depending on the number of write pulses. (b) PPF index represented as a function of time interval between twin spikes. Two identical pulses

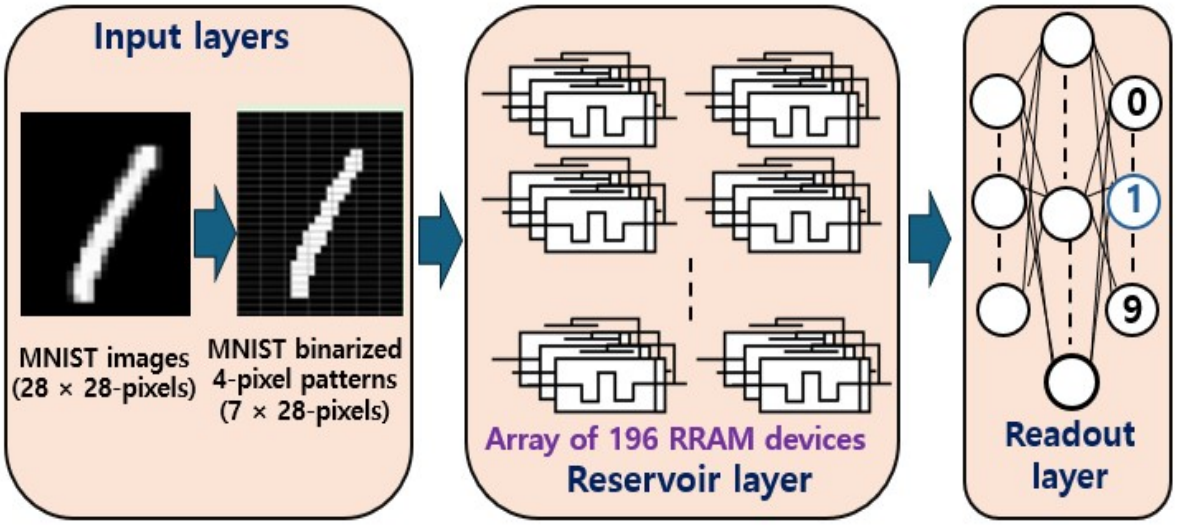

of 4 V and 500 μs duration were applied at various pulse intervals. (c) Each different EPSC Gain acquired depending on the number and amplitude of the set pulse. (d) SADP function acquired through applying 10 sequential pulses of increasing amplitude. (e) SRDP function acquired through applying 10 sequential pulses of increasing interval. For such experiment, write pulses of amplitude and width of 3.5 V and 2 ms was applied, under different numbers. Moreover, a series of read pulses were conducted to observe the current decay following the application of a stimulus at 2 V for 0.2 s. Sequential application of a small number of write pulses results in a gradual current decay as the device returns to its original HRS after short period of time. On the contrary, increasing the number of write pulses prevents the current from reverting to its initial state. During the same 0.2 s decay period, the increase in write pulses led to a gradual facilitation of current, suggesting a transition towards LTM, replicating the memory property of the biological brain whereupon the process of rehearsal or under stronger stimuli, the transition from STM to LTM occurs.

Figure S7. Schematic illustration of the pattern recognition system using reservoir computing system.

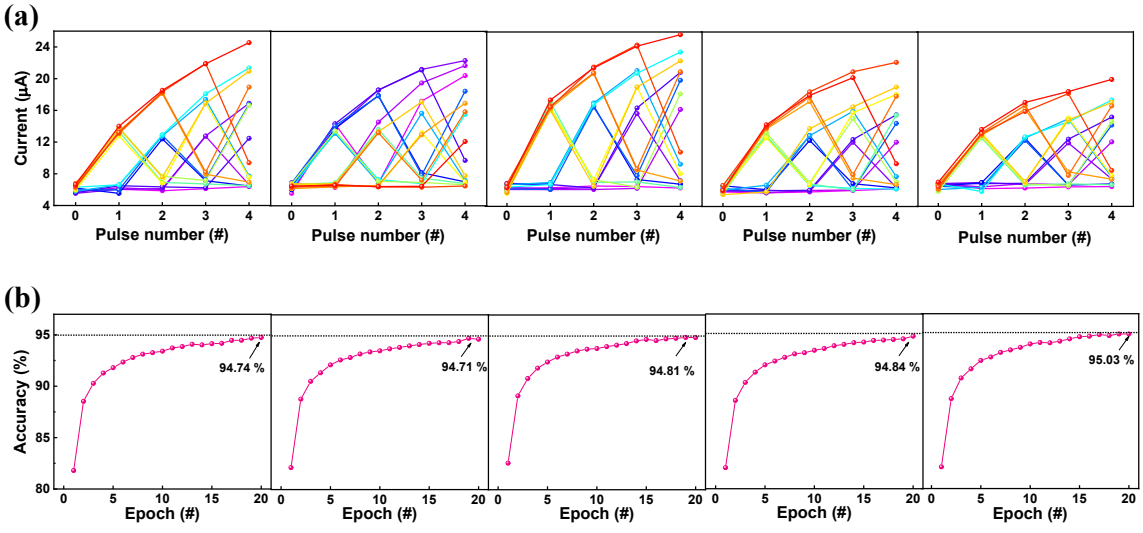

Figure S8. (a) 4-bit reservoir computing implemented from 5 different cells. (b) Pattern recognition accuracy achieved with 20 consecutive epochs applied to 5 cells.

References

[S1] W. Song, W. Wang, H. K. Lee, M. Li, V. Y. Q. Zhuo, Z. Chen, K. J. Chui, J. C. Liu, I. T. Wang, Y. Zhu and N. Singh, *Appl. Phys. Lett.*, 2019, 115, 133501.

[S2] J. H. Ryu and S. Kim, *Chaos Solitons Fractals*, 2020, 140, 110236.

[S3] S. Ali, M. Hussain, M. Ismail, M. W. Iqbal and S. Kim, *J. Alloys Compd.*, 2024, 997, 174802.

[S4] P. Jetty, U. M. Kannan and S. Jammalamadaka, *ACS Appl. Electron. Mater.*, 2024, **6**, 1992–2002.

[S5] K. C. Chuang, C. Y. Chu, H. X. Zhang, J. D. Luo, W. S. Li, Y. S. Li and H. C. Cheng, IEEE J. Electron Devices Soc., 2019, 7, 589–595.

[S6] J. Yang, H. Cho, H. Ryu, M. Ismail, C. Mahata and S. Kim, *ACS Appl. Mater. Interfaces*, 2021, **13**, 33244–33252